Volume 17
Number 37
7 October 2025
Pages 21275-21878

Nanoscale

rsc.li/nanoscale

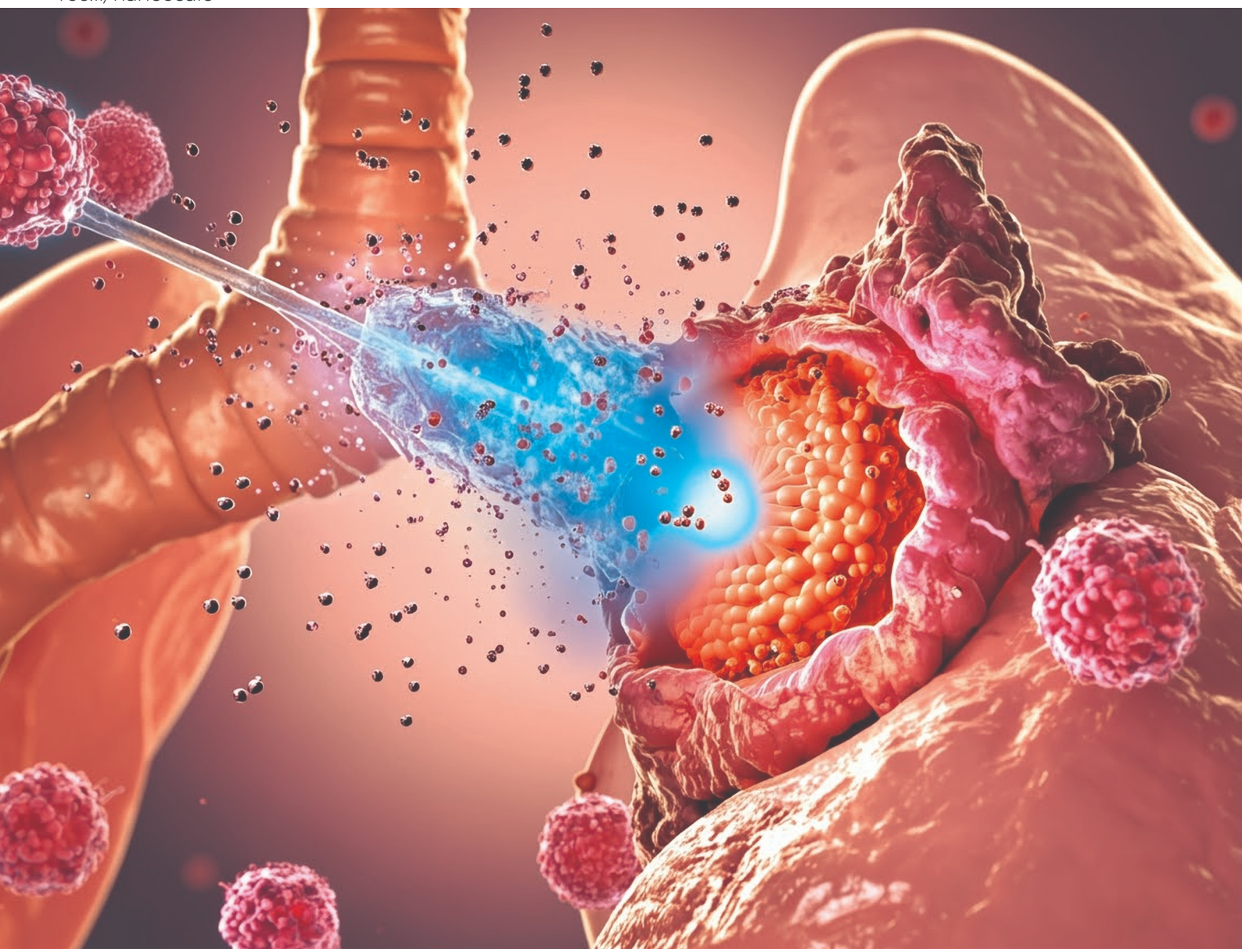

ISSN 2040-3372

ROYAL SOCIETY OF CHEMISTRY

COMMUNICATION
Jin-Ho Choy *et al.*
Transforming docetaxel delivery: lung-targeted polyphosphazene nanoparticles with enhanced safety profile

NCNST

Nanoscale

COMMUNICATION

View Article Online
View Journal | View Issue

Cite this: *Nanoscale*, 2025, **17**, 21458

Received 24th May 2025,
Accepted 20th July 2025

DOI: 10.1039/d5nr02201k

rsc.li/nanoscale

Transforming docetaxel delivery: lung-targeted polyphosphazene nanoparticles with enhanced safety profile†

Sanoj Rejinold N,[a] Geun-Woo Jin,[b] Ji Eun Oh,[c] Hye Hyun Yoo[c] and Jin-Ho Choy *[a,d]

Polyphosphazene–docetaxel conjugate (Polytaxel, PTX) represents a rationally engineered nanomedicine designed to address the limitations of conventional taxane chemotherapy. PTX exhibits improved aqueous solubility, controlled drug release, and favorable NOAEL (no observed adverse effect level) characteristics, making it a promising alternative to free docetaxel (DTX). In this study, we demonstrate that PTX achieves robust anti-tumor efficacy both *in vitro* and *in vivo*, while markedly reducing systemic toxicity compared to DTX. In an A549 xenograft mouse model, PTX suppressed tumor growth without inducing weight loss or mortality. Furthermore, *in vivo* metabolic profiling revealed a distinct biodegradation and clearance mechanism, with minimal generation of inactive or toxic metabolites. These results highlight the potential of PTX as a safe and effective drug delivery platform that combines enhanced therapeutic performance with reduced systemic burden, supporting its future clinical translation in cancer chemotherapy.

Introduction

Lung cancer is a major malignancy with a 5-year survival rate of only ~15%. The American Cancer Survey reports that 0.2 million citizens have been diagnosed with lung cancer, where 80% of reports are found as non-small-cell lung carcinoma (NSCLC) and the rest are small-cell lung carcinoma (SCLC). Currently,[1] lung cancer treatments, such as a combination of surgery, chemotherapy, and/or radiation therapy, are greatly influenced by the severity of the disease at diagnosis.[2]

Although chemotherapy is beneficial as a first-line treatment option, its non-specificity may be harmful to patients.[3–5] Conventional lung cancer chemotherapeutic approaches mainly include paclitaxel and docetaxel (DTX), which are taxane-based.[6–8] Nevertheless, DTX is fraught with dose-limiting side effects, including severe symptoms of weight loss, neutropenia, nausea, and fatigue.[9,10] Additionally, the hydrophobic nature of DTX makes it poorly aqueous-soluble, thereby limiting high-dose therapy. Mitigating such limitations to obtain better tumor targeting and efficacy through enhanced pharmacological effects without toxicity to healthy cells is a major challenge in anti-cancer therapy. Advanced nanotechnology offers enormous opportunities for the development of highly selective anti-cancer therapeutics.[11] Such revolutionary expanding techniques have been changing cancer treatment and management. Most importantly, advanced nanodrug delivery systems enable precise design of drug formulations and thereby improve the overall therapeutic efficacy of many conventional chemotherapeutic agents. Such rationally designed nanoparticles can enhance pharmacological effects and eventually enhance drug efficacy in a highly selective manner.[12–20] Here we sought to examine the therapeutic potential of our rationally designed DTX conjugated polyphosphazene-based polymer, known as polytaxel (PTX), in lung cancer. As we already reported,[21] the polyphosphazene–docetaxel (PTX) conjugate was synthesized *via* a multistep strategy beginning with the polymerization of $Cl_3P = NSiMe_3$, initiated by PCl_5 under anhydrous conditions, to yield a poly(dichlorophosphazene) backbone. Subsequent macromolecular substitution with mPEG and Boc-lysine ethyl ester afforded a PEGylated carrier polymer (CP), followed by TFA-mediated deprotection and membrane fractionation to isolate CP (M_w 30–100 kDa; ~3 nm). Separately, docetaxel (DTX) was derivatized *via* TMS protection and conjugated to *cis*-aconitic anhydride chloride (AACl), yielding an acid-sensitive prodrug intermediate. This DTX precursor was covalently conjugated to CP using TEA in THF, producing the PTX nanoconjugate, which was further functionalized with a Cy5.5 fluorophore *via* HBTU-mediated coupling. The final construct was characterized by ^1H and ^{31}P NMR spectroscopy and membrane-based molecular weight cutoff analysis.

[a]*Intelligent Nanohybrid Materials Laboratory (INML), Department of Chemistry, College of Science and Technology, Dankook University, Cheonan 31116, Republic of Korea. E-mail: sanojrejinold@dankook.ac.kr*
[b]*R&D Center, Hyundai Bioscience Co. Ltd, Seoul, 07990, Republic of Korea. E-mail: geunwoo.jin@hyundaibio.com*
[c]*College of Pharmacy, Hanyang University, Ansan, 15588, Republic of Korea*
[d]*Division of Natural Sciences, The National Academy of Sciences, Seoul 06579, Republic of Korea. E-mail: jhchoy@dankook.ac.kr*

† Electronic supplementary information (ESI) available. See DOI: https://doi.org/10.1039/d5nr02201k

PTX nanoparticles, referring to self-assembled nanostructures of polytaxel (a polymer-modified form of docetaxel), are designed to enhance solubility, prolong circulation, and enable controlled drug release. These nanoparticles demonstrated desirable pharmacokinetic profiles and favorable biodistribution patterns.[21] In contrast, conventional DTX formulations exhibited extremely high plasma concentrations exceeding the maximum therapeutic threshold, potentially leading to severe systemic side effects. In our previous study[21], PTX demonstrated effective localization within pancreatic tumors. Building on these findings, the present study investigates its application in lung cancer therapy, based on the rationale that its tumor-targeted accumulation may similarly enhance efficacy while minimizing systemic toxicity.

Results and discussion

PTX was synthesized with a step-wise process (Fig. 1) as described in our previous report[21] and further details have been provided in the ESI.† Dynamic light scattering (DLS) analysis showed that the CP complex had an average particle size of ~2.1 nm with a zeta potential of −16.6 mV, indicating small and stable structures (PDI ~ 0.366, Table S1†). Upon conjugation with docetaxel (DTX), the nanoparticle size increased to ~58 nm (PDI ~ 0.285, Table S1†) with a negative zeta potential of −30.1 mV, confirming successful drug loading and nanoparticle formation. High-Angle Annular Dark-Field imaging (HAADF) and transmission electron microscopy (TEM) images further validated the formation of uniformly spherical and monodisperse PTX nanoparticles, consistent with DLS findings. The synthesized polyphosphazene–docetaxel nanoconjugates exhibited drug content values ranging from 10.4% to 15.8%, with an average drug content of **13.2% w/w**, confirming efficient drug conjugation across all polymeric variants (Table S2†).

Furthermore, the anti-cancer efficacy of PTX was tested by evaluating the anti-proliferation activity using water-soluble tetrazolium-1 (WST-1) salt in A549 cells. Experimental results showed that PTX inhibited cell proliferation in a similar manner to DTX after 24 h (Fig. 2a), but the former had a lower effect on cell proliferation than the latter after 48 h at low con-

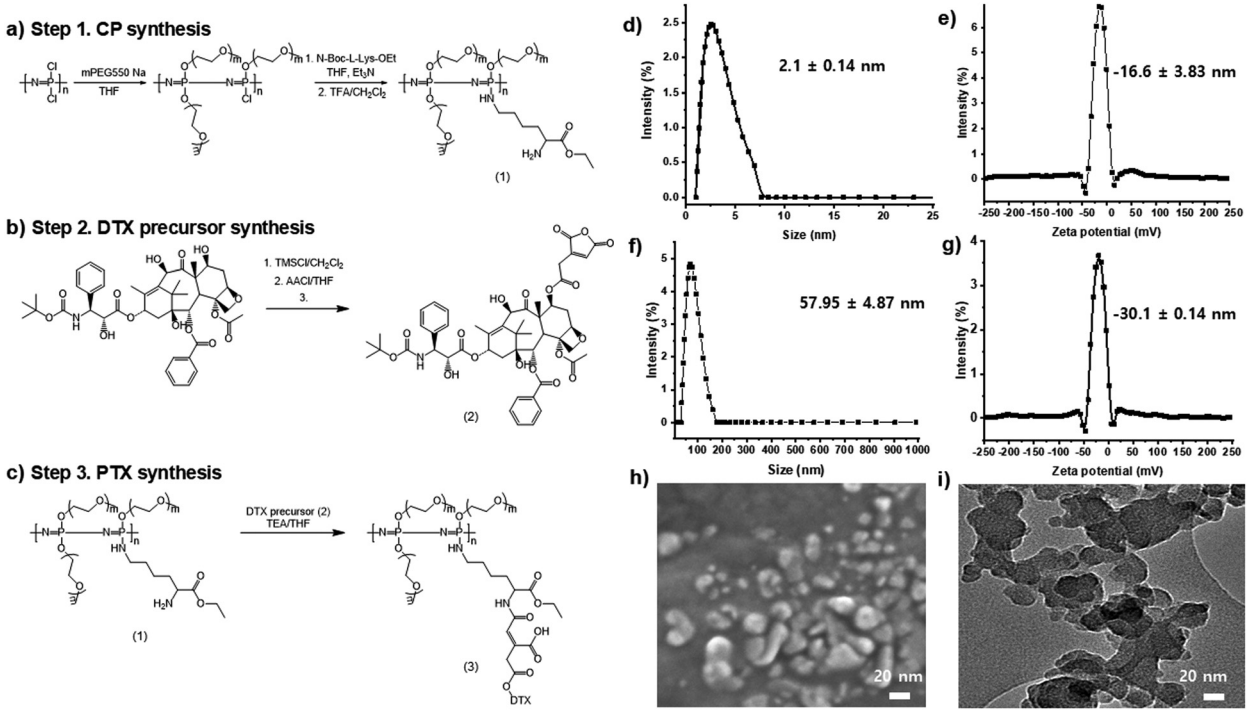

Fig. 1 Schematic illustration, synthesis route, and physicochemical characterization of polyphosphazene–docetaxel (PTX) conjugate nanoparticles. (a) Stepwise synthesis of the carrier polymer (CP): the poly(dichlorophosphazene) backbone was first modified with mPEG550 sodium salt and *N*-Boc-L-lysine ethyl ester *via* nucleophilic substitution in THF using triethylamine (Et_3N) as a base. Subsequent deprotection with trifluoroacetic acid (TFA) and CH_2Cl_2 yielded the amino-functionalized CP (**1**). (b) Synthesis of the docetaxel (DTX) precursor: the hydroxyl groups of DTX were protected using TMSCl in CH_2Cl_2, followed by reaction with activated *cis*-aconitic anhydride chloride (AACl) in THF to form an acid-cleavable linker-modified DTX intermediate (**2**). (c) Final conjugation step: the DTX precursor was covalently attached to the CP (**1**) in the presence of triethylamine (TEA) in THF, affording the polyphosphazene–DTX conjugate (**3**). (d and e) Dynamic light scattering (DLS) and Zeta potential analyses of CP showing the particle size distribution by intensity (d), with an average hydrodynamic diameter of ~2.1 ± 0.14 nm and a (e) zeta potential value of −16.6 ± 3.83 mV. (f and g) DLS and Zeta potential analyses of PTX nanoparticles showing intensity (f) distributions with an increased average particle size of ~58 nm and a (g) significant negative zeta potential value of −30.1 ± 0.14 mV, indicating successful DTX conjugation and nanoparticle formation. (h) High-Angle Annular Dark-Field (HAADF) image of PTX nanoparticles reveals a uniform spherical morphology. (i) Transmission electron microscopy (TEM) image of PTX nanoparticles, confirming their spherical shape at a scale of 20 nm.[21]

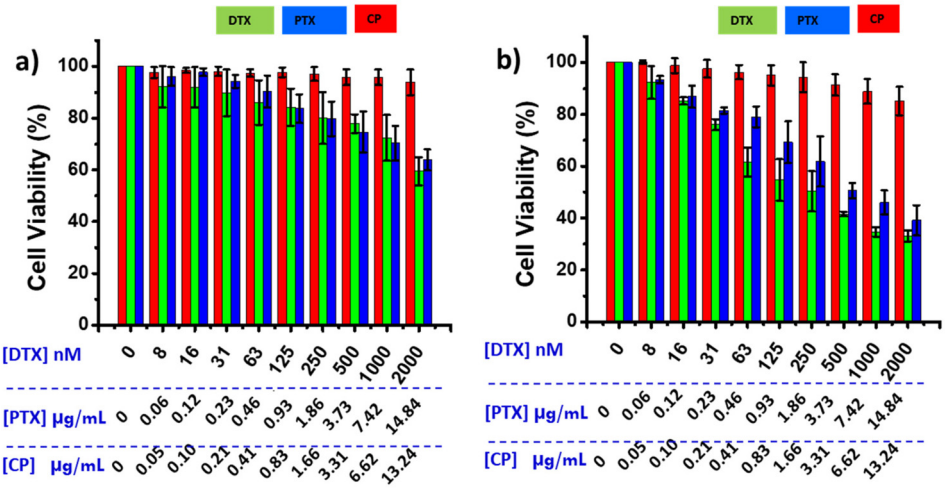

Fig. 2 Cell proliferation by the WST-1 assay of A549 cells treated with DTX, PTX, or CP after 24 h (a) and 48 h (b) of incubation, respectively.

centrations (Fig. 2b). It is worth noting that nanocarriers had no effect on cell proliferation, indicating their biological safety. Next, we studied the metabolites of PTX and compared them with those of DTX (Fig. S1 and S2†). The metabolites for PTX were analysed using human, monkey, dog, rat and mouse microsomes.[22] Comparative metabolic profiles of DTX and PTX among human, monkey, dog, rat and mouse liver microsomes are shown in Fig. 3a. The main metabolites of DTX and PTX were the same as M1, M2 and M3. In DTX, the production of M2 was predominant. In PTX, free DTX was hardly detected, and most of it was metabolized to M1 and M3. Also, in DTX, the ratio of metabolites generated compared to the parent was low, but in the case of PTX, it showed the opposite patterns. A very small amount of DTX was isolated and metabolized from PTX. As a result, DTX and PTX differed in metabolite production rates. The data from the study support that the released DTX from PTX undergoes the same metabolism pathway, with DTX yielding the same metabolites (Fig. 3).[23]

As shown in Fig. 3, docetaxel (DTX) undergoes extensive biotransformation, primarily forming the M2 metabolite, which is subsequently converted into M1 and M3. These metabolic conversions are characteristic of hepatic cytochrome P450-mediated hydroxylation and oxidation pathways, which are commonly linked to reduced drug efficacy and heightened systemic toxicity. Importantly, literature reports indicate that major DTX metabolites such as M1 and M3 exhibit significantly diminished or no anti-cancer activity.[24] This highlights a critical pharmacokinetic liability: the rapid metabolism of DTX may severely limit its therapeutic potential *in vivo*, even though the *in vitro* anti-proliferative effects are largely attributed to the parent (intact) drug. In contrast, the metabolic profile of PTX (Fig. 3a, right panel) demonstrated substantially attenuated bioconversion, reflecting enhanced metabolic stability. The limited generation of secondary metabolites suggests prolonged systemic retention of the parent compound, which is beneficial for maintaining sustained therapeutic activity at the tumor site. These findings support our delivery strategy aimed at protecting the intact drug and prolonging its circulation time, thereby enhancing both efficacy and safety, as further evaluated in a lung cancer model.

Prior to the *in vivo* studies, an extended *in vitro* release assessment was conducted to evaluate the long-term drug release behaviour of the PTX nanoparticles under physiological (pH 7.4) and tumor-mimicking acidic (pH 5.0) conditions. The release profile revealed a highly sustained and controlled release of DTX over approximately 1500 hours (~62.5 days), without the initial burst effect typically associated with conventional formulations (Fig. S3†).

At pH 7.4, simulating physiological conditions in systemic circulation, the nanoparticles exhibited a sustained, diffusion-controlled release of DTX throughout the study period. In contrast, at pH 5.0—mimicking the acidic tumor microenvironment and intracellular endosomal compartments—a moderately faster release was observed, indicating a pH-responsive behavior of the anionic matrix that enhances drug liberation under acidic conditions. This suggests that the matrix facilitates enhanced drug release in environments typical of tumor tissues, providing a targeted therapeutic advantage.

This prolonged and environment-responsive release is particularly advantageous for lung cancer therapy. It enables steady therapeutic levels of DTX in circulation while promoting enhanced drug liberation within the tumor milieu. The sustained release not only supports reduced dosing frequency and improved patient compliance but also aligns with enhanced permeability and retention (EPR)-driven accumulation in non-small cell lung cancer (NSCLC). Furthermore, the anionic surface likely contributes to stealth properties, minimizing premature opsonization and clearance by the mononuclear phagocyte system (MPS), thereby extending systemic circulation and improving tumor-targeted drug delivery.[25]

Collectively, these findings highlight the potential of anionic PTX nanoparticles to transform current chemotherapeutic regimens by enabling precision drug delivery, minimizing systemic side effects, and prolonging the

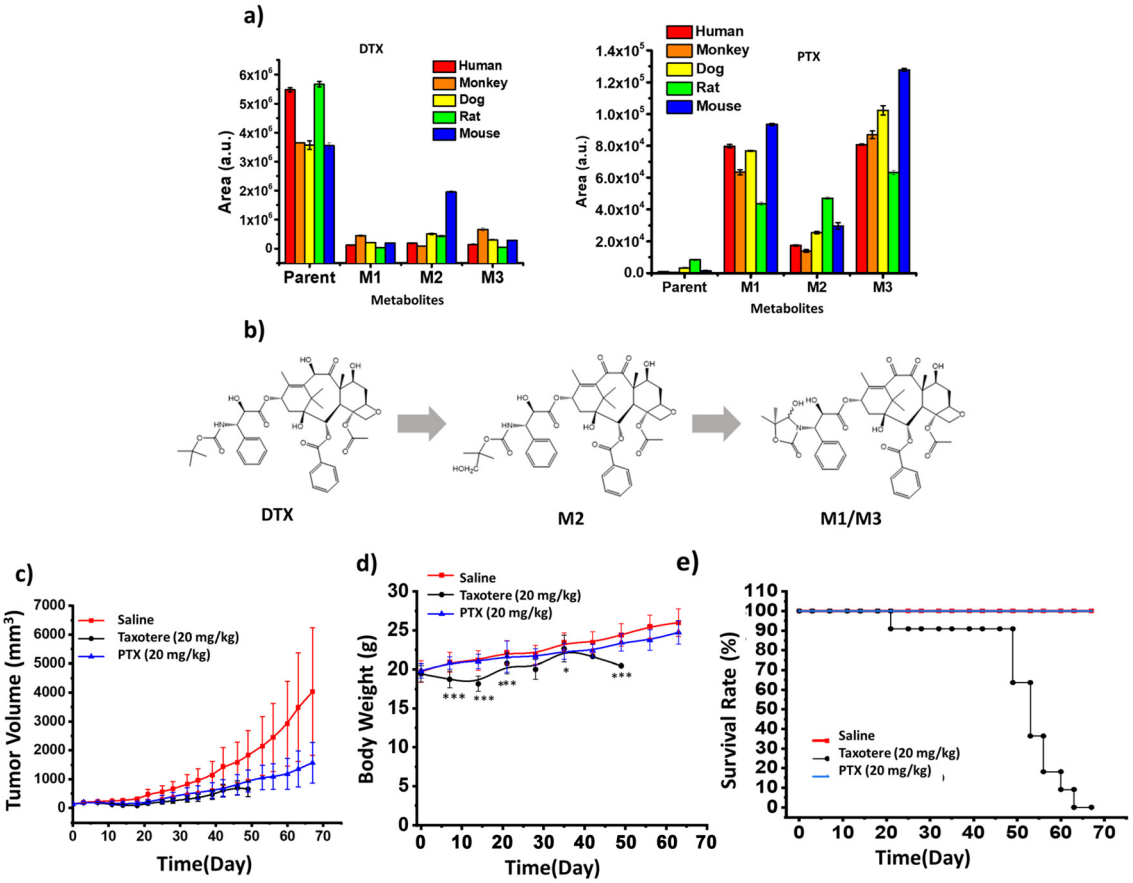

Fig. 3 (a) Comparative analysis of DTX and PTX metabolism across different tissue types and metabolite pathways. Bar graphs represent the relative abundance of various DTX metabolites in liver microsomes from five species: human (red), monkey (orange), dog (yellow), rat (green), and mouse (blue). (b) The metabolic pathway at the bottom illustrates the sequential biotransformation of DTX into its major metabolites M2, followed by M1 and M3. The data reveal species-specific differences in DTX metabolism, with liver microsomes primarily generating M2 and minor metabolites, whereas intestinal microsomes show enhanced conversion into M1/M3. (c–e) *In vivo* antitumor efficacy of Taxotere (20 mg kg^{-1}) and PTX (20 mg kg^{-1}) compared to saline in tumor-bearing mice. (c) Tumor volume measurements show that Taxotere-treated mice exhibited rapid tumor growth, similar to the saline group, while PTX treatment significantly suppressed tumor progression. (d) The body weight remained stable across all groups, indicating no major systemic toxicity. (e) Survival analysis revealed a decline in survival in the Taxotere group before day 50, dropping to ~60–70%, while the PTX group maintained 100% survival. No notable change in general activity scores was observed. Due to the combination of uncontrolled tumor growth and reduced survival, Taxotere evaluation was ethically terminated at day 50 in accordance with animal welfare guidelines in the lung cancer model. Data were expressed as mean ± S.D. A significant difference at the ***$P < 0.001$/*$P < 0.01$ level compared to the saline-treated group (control) ($n = 11$).

therapeutic window—thus offering a highly translational approach for the sustained treatment of aggressive pulmonary malignancies.

The *in vivo* antitumor efficacy of PTX on A549 tumor-bearing athymic nude mice was compared with intact DTX. DTX or PTX was administered at a dose of 20 mg kg^{-1} based on the DTX content (3 times per week: on days 1, 4, and 7). The saline group was set as a negative control.

The antitumor efficacy of polytaxel (PTX) was found to be comparable to that of docetaxel (DTX), as evidenced by similar tumor growth inhibition rates in the lung cancer xenograft model (Fig. 3c). However, a marked difference emerged in terms of systemic toxicity between the two treatment groups. Mice treated with DTX exhibited substantial body weight loss, indicative of significant treatment-related toxicity. In contrast, the PTX-treated group maintained stable body weights throughout the 60-day study period, reflecting an improved safety profile (Fig. 3d). Notably, the PTX group also achieved a 100% survival rate with no observable signs of acute or delayed toxicity, underscoring its superior *in vivo* tolerability and therapeutic index (Fig. 3e). These findings highlight the potential of the PTX formulation to deliver effective lung cancer therapy with minimal systemic side effects. Taken together, the metabolic stability and improved therapeutic index of PTX position it as a compelling candidate for further development using nanotechnology-enabled delivery platforms. By leveraging nanoscale encapsulation or self-assembled systems, it is feasible to enhance the bioavailability, tumor targeting ability, and retention of PTX while minimizing systemic exposure. These data support the rationale for deploying PTX within nanohy-

brid constructs as a sustainable and targeted strategy for lung cancer therapy.

Conclusions

A polyphosphazene-based drug conjugate of docetaxel (PTX) was rationally engineered to assess its therapeutic efficacy against lung cancer in both *in vitro* and *in vivo* models. The results demonstrate that PTX offers significant anti-tumor activity at low doses, with minimal systemic toxicity, supporting its potential as a NOAEL (No Observed Adverse Effect Level) cancer therapeutic agent. In an A549 xenograft model, PTX markedly suppressed tumor growth while avoiding common docetaxel-associated adverse effects such as body weight loss and mortality. These findings highlight PTX as a promising candidate for lung cancer treatment, combining enhanced efficacy with a favourable safety profile.

Author contributions

N. Sanoj Rejinold: methodology, investigation, data curation, writing – original draft, and visualization. Geun-Woo Jin: formal analysis, validation, resources, investigation, and data interpretation. Ji Eun Oh: methodology, experimental support, cell culture studies, and data analysis. Hye Hyun Yoo: supervision (*in vivo* studies), pharmacokinetic analysis, and review & editing. Jin-Ho Choy: conceptualization, supervision, project administration, funding acquisition, writing – review & editing, and final approval of the manuscript.

Conflicts of interest

There are no conflicts to declare.

Data availability

The data that support the findings of this study are available within the article and its ESI.† Additional raw data and materials are available from the corresponding author upon reasonable request.

Acknowledgements

This study was supported by the National Research Foundation of Korea (NRF) (Grant Nos. RS-2023-00245466 and RS-2023-00242339).

References

1 D. Subotic, L. Molins, I. Soldatovic, D. Moskovljevic, L. Collado and J. Hernández, *World J. Surg. Oncol.*, 2018, **16**, 98.
2 R. L. Siegel, T. B. Kratzer, A. N. Giaquinto, H. Sung and A. Jemal, *CA-Cancer J. Clin.*, 2025, **75**, 10–45.
3 A. Zafar, S. Khatoon, M. J. Khan, J. Abu and A. Naeem, *Discover Oncol.*, 2025, **16**, 607.
4 J. Venkataraman and K. Mokbel, *Breast Cancer Res. Treat.*, 2025, **212**, 183–184.
5 W. Grisold and A. Grisold, *Curr. Med. Res. Opin.*, 2017, **33**, 1291–1292.
6 M. Lambertini and B. Nordenskjold, *Lancet Reg. Health Eur.*, 2025, **49**, 101212.
7 O. Fiste, L. Vamvakas, P. Katsaounis, N. Vardakis, S. Kallianteri, V. Georgoulias and A. Karampeazis, *J. Geriatr. Oncol.*, 2025, **16**, 102184.
8 R. L. Li, L. X. Bai, Y. Liu, A. L. Yang, L. Chen, F. Y. Zhao, L. Zhang and J. E. Liu, *Eur. J. Oncol. Nurs.*, 2025, **74**, 102758.
9 M. Bathara, T. Date, D. Chaudhari, R. Ghadi, K. Kuche and S. Jain, *Mol. Pharm.*, 2020, **17**, 2473–2486.
10 J. Choi, E. Ko, H. K. Chung, J. H. Lee, E. J. Ju, H. K. Lim, I. Park, K. S. Kim, J. H. Lee, W. C. Son, J. S. Lee, J. Jung, S. Y. Jeong, S. Y. Song and E. K. Choi, *Int. J. Nanomed.*, 2015, **10**, 6121–6132.
11 S. Islam, M. M. S. Ahmed, M. A. Islam, N. Hossain and M. A. Chowdhury, *Results Surf. Interfaces*, 2025, **19**, 100529.
12 M. Chai, S. Wang, Y. Chen, X. Pei and X. Zhen, *Front. Bioeng. Biotechnol.*, 2025, **13**, 1582659.
13 C. Guo, L. Lin, Y. Wang, J. Jing, Q. Gong and K. Luo, *Theranostics*, 2025, **15**, 5440–5480.
14 B. Song, L. Shuang, S. Zhang, C. Tong, Q. Chen, Y. Li, M. Hao, W. Niu and C. H. Jin, *PeerJ*, 2025, **13**, e19332.
15 X. Wu, M. Hu, Y. Cai, F. Jia, Y. Ye, N. Yu, M. Chen and K. Wang, *Adv. Ophthalmol. Pract. Res.*, 2025, **5**, 124–134.
16 A. Faraji-Barhagh, S. Jahandar-Lashaki, R. J. Esfahlan and E. Alizadeh, *Mol. Biol. Rep.*, 2025, **52**, 369.
17 A. Pontoriero, P. Critelli, M. Zeppieri, A. Bosurgi, S. Guercio, M. Caffo, F. F. Angileri, S. Parisi, S. Lavalle and S. Pergolizzi, *World J Clin Cases*, 2025, **13**, 101719.
18 X. Shao, X. Zhao, B. Wang, J. Fan, J. Wang and H. An, *Theranostics*, 2025, **15**, 1689–1714.
19 Y. Deng, L. Liu, Y. Li, H. Ma, C. Li, K. Yan, J. Tian and C. Li, *Drug Delivery Transl. Res.*, 2025, **15**(8), 2924–2940.
20 X. J. Dai, W. J. Li, D. D. Xie, B. X. Liu, L. Gong and H. H. Han, *Small*, 2025, **21**, e2410030.
21 G.-W. Jin, G. Choi, H. Piao, N. S. Rejinold, S. Asahina, S.-J. Choi, H. J. Lee and J.-H. Choy, *J. Mater. Chem. B*, 2023, **11**, 565–575.
22 H. Zhang, N. Gao, X. Tian, T. Liu, Y. Fang, J. Zhou, Q. Wen, B. Xu, B. Qi, J. Gao, H. Li, L. Jia and H. Qiao, *Sci. Rep.*, 2015, **5**, 17671.
23 M. A. C. Vermunt, M. van Nuland, L. T. van der Heijden, H. Rosing, J. H. Beijnen and A. M. Bergman, *Cancer Chemother. Pharmacol.*, 2022, **89**, 785–793.
24 L. van Zuylen, J. Verweij, K. Nooter, E. Brouwer, G. Stoter and A. Sparreboom, *Clin. Cancer Res.*, 2000, **6**, 2598–2603.
25 S. Y. Fam, C. F. Chee, C. Y. Yong, K. L. Ho, A. R. Mariatulqabtiah and W. S. Tan, *Nanomaterials*, 2020, **10**(4), 787.

